Exotic magnetism and spin-orbit-assisted Mott insulating state in a 3*d*-5*d* double perovskite

A. S. Cavichini,[1] M. T. Orlando,[1] J. B. Depianti,[1] J. L. Passamai, Jr.,[1] F. Damay,[2] F. Porcher,[2] and E. Granado[3]
[1]*Universidade Federal do Espírito Santo, Vitória, Espírito Santo 29075-910, Brazil*
[2]*Laboratoire Léon Brillouin, CEA, Centre National de la Recherche Scientifique, CE-Saclay, 91191 Gif-sur-Yvette, France*
[3]*"Gleb Wataghin" Institute of Physics, University of Campinas - UNICAMP, Campinas, São Paulo 13083-859, Brazil*

(Received 12 December 2017; revised manuscript received 15 February 2018; published 28 February 2018)

The magnetic structure of Ca_2MnReO_6 double perovskite is investigated by neutron powder diffraction and bulk magnetization, showing dominant noncollinear Mn magnetic moments [4.35(7) μ_B] that are orthogonally aligned with the small Re moments [0.22(4) μ_B]. *Ab initio* electronic structure calculations show that the strong spin-orbit coupling for Re 5*d* electrons combined with a relatively modest on-site Coulomb repulsion ($U_{\rm eff}^{Re} \gtrsim 0.6$ eV) is sufficient to render this material insulating. This is a rare example of spin-orbit-assisted Mott insulator outside the realm of iridates, with remarkable magnetic properties.

DOI: 10.1103/PhysRevB.97.054431

I. INTRODUCTION

The identification of a spin-orbit entangled Mott insulating state in Sr_2IrO_4 triggered a quest for novel quantum phases in 5*d*-based materials [1–5]. In such systems with strong spin-orbit coupling (SOC), a Heisenberg Hamiltonian is not sufficient to describe the magnetic ground states and excitations, therefore alternative treatments may be necessary to describe the effect of anisotropic exchange interactions [5]. Also, the electronic correlations in 5*d* systems are relatively weak, and the atomic moments are normally small compared to the 3*d* counterparts. Alternating 3*d* and 5*d* ions in an ordered double perovskite structure offers a possible pathway to investigate ground states arising from the combination of strong SOC in 5*d* ions and strong electronic correlation in 3*d* ions. An example is Ca_2MnReO_6 (CMRO), which was previously described as a ferromagnetic insulator with a small saturation magnetization of 0.9 μ_B/f.u. and coercive field of 4 T [6], also showing Mn valence close to +2 [7,8]. In this paper, an unusual magnetic structure is demonstrated, with dominating Mn moments forming a largely canted sublattice, while weak Re moments are orthogonally aligned with Mn moments. Electronic structure calculations reveal that a combination of Re SOC and electronic correlations renders this material insulating, revealing a determinant role of the Re moments to the overall electronic and magnetic behavior of this material.

II. EXPERIMENTAL AND COMPUTATIONAL DETAILS

The polycrystalline CMRO sample was synthesized by solid state reaction [8]. dc-magnetization and magnetic susceptibility measurements were performed in a commercial platform. Cold neutron powder diffraction (c-NPD) measurements were taken at the *G*4-1 instrument of Laboratorie Léon Brillouin (LLB), using a highly oriented pyrolytic graphite (HOPG) monochromator with vertical focusing and $\lambda = 2.43$ Å, a two-axis diffractometer and a BF_3 multicell detector with 80° aperture and 0.1° resolution. High resolution thermal neutron powder diffraction (t-NPD) measurements were also taken, and details are given in the Appendix. The sample was kept sealed under He atmosphere in a vanadium can and mounted into the cold finger of a LHe cryostat. The powder diffraction data were independently analyzed using the Fullprof [9] and GSAS [10] suites, with similar results. The refined degree of Mn/Re antisite disorder is 0.6(7)%. The Re^{6+} magnetic form factor was taken from Ref. [11]. *ab initio* electronic structure calculations were carried out with relativistic density-functional theory using the QUANTUM ESPRESSO package [12] under the generalized gradient approximation, using the Perdew, Burke, and Enzerhof exchange-correlation potential [13] and the projector augmented wave method [14,15]. The energy cutoffs for the wave functions and charge density were 57 and 702 Ry, respectively. The atomic-projected magnetizations were obtained by a self-consistent field (scf) calculation using a $6 \times 6 \times 4$ Monkhorst-Pack grid of k points. The density of states was obtained from a subsequent non-scf calculation with a denser $12 \times 12 \times 8$ k-point grid, using 0.03 eV Gaussian broadening. The experimental crystal structure was employed as input of our calculations.

III. RESULTS AND ANALYSIS

A. Bulk magnetization and *dc*-magnetic susceptibility

Figure 1(a) shows $M(T)$ curves of CMRO for $H = 0.1$ and 5 T. The zero-field cooled (ZFC) magnetization with $H = 0.1$ T is negligible up to 70 K, shows a peak at $T_{\rm max} = 100$ K, and a paramagnetic transition at $T_c = 121$ K. The $H = 0.1$ T field-cooling (FC) curve follows the ZFC one above $T_{\rm max}$, retaining a significant magnetization (∼0.5 μ_B/f.u.) below $T_{\rm max}$. The $H = 5$ T FC magnetization also shows a transition at T_c and a peak at $T_{\rm max}$, reaching $M = 0.7$ μ_B at the base T. The inverse magnetic susceptibility χ^{-1} taken with $H = 0.1$ T, also shown in Fig. 1(a), follows a Curie-Weiss law in the high-T limit, $\chi^{-1} = (T - \theta_{CW})/C$ with $\theta_{CW} = 70$ K and $C = 1.42 \times 10^{-2}$ Km^3/mol, with relevant deviations from this law below ∼150 K [see Fig. 1(a)]. The positive value of θ_{CW} indicates mostly ferromagnetic exchange interactions between the dominant magnetic

 ©2018 American Physical Society

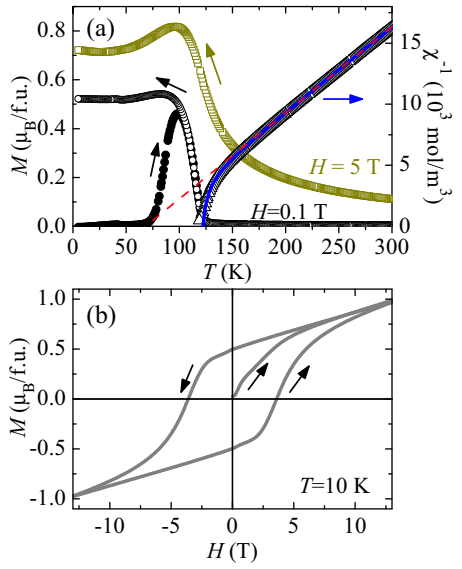

FIG. 1. (a) T dependence of the dc magnetization of Ca_2MnReO_6 under warming at $H = 0.1$ T after zero-field cooling (ZFC, filled circles), field cooling (FC) at $H = 0.1$ T (empty circles), and FC at $H = 5$ T (empty squares). The inverse magnetic susceptibility obtained from FC magnetization data at $H = 0.1$ T is shown as empty triangles, together with fits to the Curie-Weiss law (dashed line) and the two-sublattice paramagnetic model (solid line, see text). (b) $M \times H$ loop taken at $T = 10$ K after ZFC.

moments. Alternatively, a fit to a two-sublattice paramagnetic model, $\chi^{-1} = T/C_m + 1/\chi_0 - b/(T - \theta)$ (Ref. [16]), yields excellent agreement with the data above T_c, with fitting parameters $C_m = 1.45 \times 10^{-2}$ K m^3/mol, $\chi_0 = 2.36 \times 10^{-4}$ m^3/mol, $b = 1.84 \times 10^4$ K.mol/m^3, and $\theta = 118$ K. The $M \times H$ loop taken at $T = 10$ K after ZFC is given in Fig. 1(b), showing a squared curve with large coercive field $H_c = 4$ T, characteristic of significant magnetocrystalline coupling, and remnant magnetization $M_{\rm rem} = 0.5\ \mu_B$/f.u., in line with Ref. [6].

B. Neutron powder diffraction

Figure 2(a) shows the c-NPD profile of CMRO at $T = 300$ K. t-NPD data are shown in the Appendix. The intensities could be well modeled by a monoclinic double perovskite structure with space group $P2_1/n$, as indicated by the solid lines of Fig. 2(a). Refined structural parameters at selected T, using t-NPD data, are given in Tables I and II. The T dependence of the refined lattice parameters is shown in Fig. 3(a). An anomalous contraction of c and expansion of b are observed on cooling below T_c.

Figure 2(b) shows the c-NPD profile of CMRO at $T = 2$ K. Additional intensities due to magnetic ordering are observed at integer (hkl) positions, showing that the magnetic unit cell coincides with the chemical one. In principle, the magnetic (Shubnikov) groups $P2_1/n$ and $P2_1'/n'$ are allowed with nonzero magnetic moments on Mn or Re sites. These magnetic groups accommodate both ferromagnetic (FM) and A-type layered antiferromagnetic (A-AFM) components. In the unprimed group, the M_x and M_z magnetization components of Mn and Re ions show an A-AFM ordering and M_y is FM,

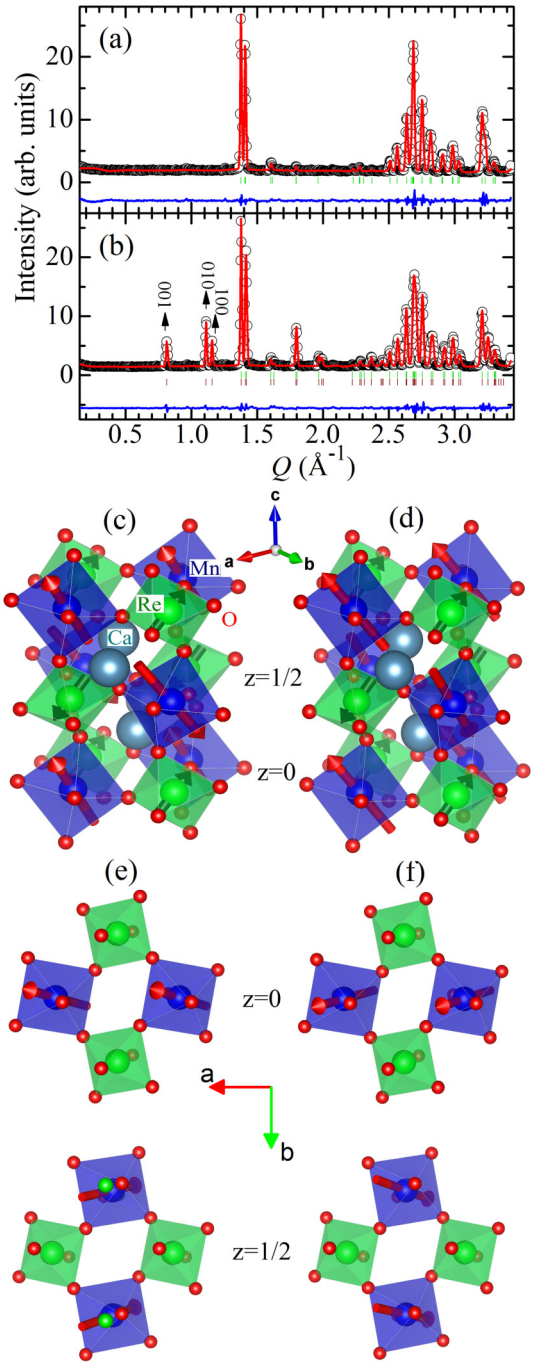

FIG. 2. Observed cold neutron powder diffraction profile of CMRO at $T = 300$ K (a) and $T = 2$ K (b) (empty circles). The calculated profiles for a monoclinic double perovskite structure and noncollinear Mn and Re magnetic moments at 2 K (see text) are shown as solid lines. The difference curves (dark solid line) are displayed at the bottom of each figure. The reflection positions are indicated by short vertical lines for both the nuclear [(a) and (b)] and magnetic [(b), lower vertical lines] structures. (c),(d) Representations of the two possible magnetic structures at $T = 2$ K (arrows), yielding identical magnetic Bragg intensities. The magnitude of the weak Re moment is exaggerated for clarity. (e),(f) *ab*-plane projections of the representations shown in (c),(d). Re moments are not displayed here. Note that in the structure of (c) and (e) the Mn moments follow the tilting pattern of the MnO_6 octahedra, contrary to the structure shown in (d) and (f).

TABLE I. Lattice parameters, atomic coordinates, and thermal factors of Ca_2MnReO_6 in three distinct temperatures using thermal neutron powder diffraction data (space group $P2_1/n$). The x, y, and z coordinates for Mn and Re are 1/2, 0, 1/2 and 1/2, 0, 0, respectively. The fitting R factors are also given.

	10 K	150 K	300 K
a (Å)	5.4250(10)	5.4238(9)	5.4336(10)
b (Å)	5.6448(10)	5.6308(10)	5.6285(10)
c (Å)	7.7165(14)	7.7473(14)	7.7610(14)
β (Å)	90.2816(15)	90.2176(12)	90.1744(12)
Cell Vol. (Å^3)	236.30(7)	236.60(7)	237.35(7)
Ca			
x	0.4873(3)	0.4879(8)	0.4887(8)
y	0.5544(6)	0.5541(6)	0.5534(7)
z	0.2531(5)	0.2542(5)	0.2531(6)
B (Å^2)	0.29(1)	0.46(1)	0.8(1)
Mn/Re			
B (Å^2)	0.06(5)	0.01(4)	0.19(4)
O1			
x	0.3182(6)	0.3193(6)	0.3190(6)
y	0.2811(6)	0.2819(6)	0.2817(6)
z	0.0563(4)	0.0549(4)	0.0532(5)
B (Å^2)	0.82(4)	0.93(4)	1.07(4)
O2			
x	0.2112(6)	0.2114(6)	0.2130(6)
y	0.8119(6)	0.8135(5)	0.8129(6)
z	0.0484(4)	0.0480(4))	0.0474(5)
B (Å^2)	0.82(4)	0.93(4)	1.07(4)
O3			
x	0.5985(6)	0.5973(6)	0.5974(6)
y	−0.0312(6)	−0.0321(6)	−0.0326(6)
z	0.2322(4)	0.2348(4)	0.2350(4)
B (Å^2)	0.82(4)	0.93(4)	1.07(4)
R_p (%)	4.17	3.83	3.60
R_{wp} (%)	3.18	2.88	2.78
χ^2	6.01	5.07	4.31

while for the primed group M_x and M_z are FM components and M_y shows an A-AFM stacking. The significant monoclinic distortion of CMRO allows for an unambiguous determination of the magnetic group, in contrast to the previously studied case of Sr_2MnReO_6 with a quasicubic cell [11,17]. In fact, the

TABLE II. (Mn,Re)-O bond distances and Mn-O-Re bond angles extracted from the data of Table I.

	10 K	150 K	300 K
Mn-O_1 (Å)	2.165(4)	2.164(4)	2.163(4)
Mn-O_2 (Å)	2.133(3)	2.137(3)	2.131(4)
Mn-O_3 (Å)	2.144(4)	2.131(4)	2.133(4)
Re-O_1 (Å)	1.919(4)	1.914(4)	1.912(4)
Re-O_2 (Å)	1.931(4)	1.922(4)	1.918(4)
Re-O_3 (Å)	1.876(4)	1.901(4)	1.906(4)
Mn-O_1-Re (°)	146.77(18)	146.82(18)	147.4(2)
Mn-O_2-Re (°)	148.87(17)	148.69(17)	149.20(18)
Mn-O_3-Re (°)	147.33(18)	147.76(18)	147.69(18)

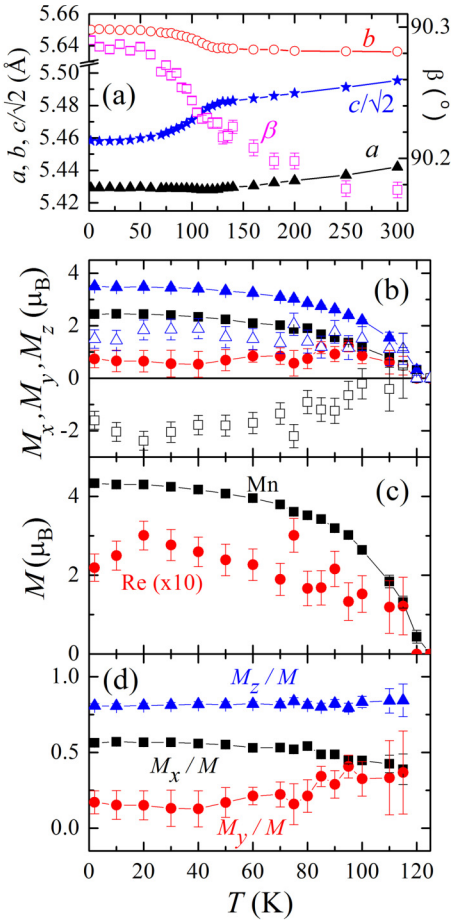

FIG. 3. T dependence of (a) lattice parameters, (b) M_x(Mn) (filled squares), M_y(Mn) (filled circles), M_z(Mn) (filled triangles), M_x(Re) ×10 (empty squares), and M_z(Re) ×10 (open triangles), (c) total Mn and Re moments, and (d) direction cosines M_i/M of the Mn moments.

presence of a strong (010) magnetic reflection, clearly separated from (100) [see Fig. 2(b)], shows that the A-AFM moments are not oriented along b, and therefore the $P2_1/n$ magnetic group is the correct one for CMRO. Still, two possible magnetic structures provide exactly the same magnetic Bragg intensities. Formally, they differ by reversing the sign of the small FM component M_y (Mn). In the magnetic structure of Figs. 2(c) and 2(e), the canted Mn moments follow the tilts of the MnO_6 octahedra around the c axis, always pointing approximately towards an octahedral face, while in Figs. 2(d) and 2(f) the canting of the Mn moments is off-phase with respect to the MnO_6 tilting pattern. At $T = 2$ K, the Mn/Re moment vectors are $[2.41(3), \pm 0.8(3), 3.53(3)]/[-0.16(4), 0, 0.15(4)]$ μ_B at $z = 0$ in Figs. 2(c) and 2(d), yielding total Mn/Re atomic moments of 4.35(7)/0.22(4) μ_B. The refined M_y (Mn) is consistent with the FM moment found in bulk magnetization measurements (see Fig. 1). Due to the weakness of the Re moment, its component along b, i.e., its minor contribution to the already small overall FM signal, could not be obtained, being fixed at zero. Figure 2(b) shows the fitting of c-NPD data to the model described above.

Figure 3(b) shows the T dependence of the Mn and Re moment components, while the total moments are given in Fig. 3(c). Both Mn and Re total moments decrease on warming,

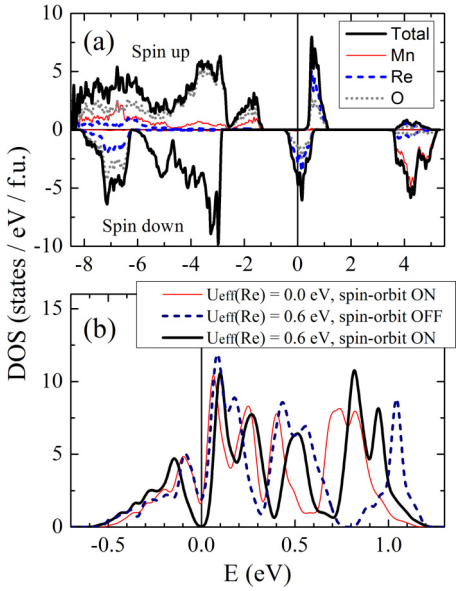

FIG. 4. (a) Mn $3d$, Re $5d$, O $2p$ and total density of states (DOS), taken for a collinear calculation without Re spin-orbit coupling and using $U(\mathrm{Mn}) = 6.9$ eV, $J(\mathrm{Mn}) = 0.86$ eV, $U(\mathrm{Re}) = J(\mathrm{Re}) = 0$, yielding a ferrimagnetic ground state. Positive and negative values refer to spin up and spin down DOS, respectively. (b) Total DOS nearby the Fermi level for calculations with and without Re spin-orbit coupling, and with and without an effective on-site Coulomb repulsion $U_{\mathrm{eff}}(\mathrm{Re}) = 0.6$ eV ($U(\mathrm{Re}) = 1.3$ eV, $J(\mathrm{Re}) = 0.7$ eV). The DOS for the collinear calculation (spin-orbit OFF) in (b) correspond to an A-AFM metastable state for the Mn moments.

critically approaching zero at $T_c = 121$ K, consistent with bulk magnetization data. Notice that $M_y(\mathrm{Mn})$ increases slightly between ~80 and 100 K, reaching $M_y(\mathrm{Mn}) = 1.2(2)\ \mu_B$ at 95 K, consistently with the magnetization maximum found in this T range [see Fig. 1(a)]. This effect is analyzed in terms of direction cosines [see Fig. 3(d)], where the relative weight of the FM component $M_y/M(\mathrm{Mn})$ increases above 80 K at expense of M_x/M, indicating a moment rotation around the c axis as $T \to T_c$.

C. Electronic structure calculations

To gain insight into the origin of the exotic magnetic structure of CMRO, *ab initio* electronic structure calculations were performed. Figure 4(a) shows the total and atom-projected density of states near the Fermi level ($E = 0$) given by a preliminary calculation with collinear magnetic moments using Coulomb (U) and exchange (J) parameters $U(\mathrm{Mn}) = 6.9$ eV, $J(\mathrm{Mn}) = 0.86$ eV (Ref. [18]), $U(\mathrm{Re}) = J(\mathrm{Re}) = 0$, and without considering SOC. With such parameters, the ground state is found to be half metallic with ferrimagnetic (FiM) ordering of Mn and Re moments. The energy levels at the vicinity of $E = 0$ show mostly Re $5d$ character, with significant mixing with O $2p$ levels but negligible participation of Mn $3d$ states. An alternative calculation performed with initial atomic magnetization defining an A-AFM structure converged into a metastable A-AFM state, with higher energy with respect to the FiM ground state ($E_{\mathrm{AFM}} - E_{\mathrm{FiM}} = 51$ meV/f.u.). The energy difference between the A-AFM and FiM states decreases by increasing the Re on-site Coulomb parameters, with a crossover to an A-AFM ground state for $U_{\mathrm{eff}}(\mathrm{Re}) > 2.2$ eV. Inclusion of Re SOC has a large impact in the electronic structure near $E = 0$. Figure 4(b) shows the total DOS at the vicinity of $E = 0$, with and without Re SOC and $5d$ on-site correlation. Remarkably, a relatively weak Re correlation [$U_{\mathrm{eff}}(\mathrm{Re}) = 0.6$ eV] in the presence of Re SOC is sufficient to open a gap in the DOS at $E = 0$, rendering the material insulating. Instead, if SOC is not considered, the energy gap is not formed for realistic values of $U_{\mathrm{eff}}(\mathrm{Re}) < 1.5$ eV. Therefore, this material can be classified as a spin-orbit-assisted Mott insulator, in similarity to Sr_2IrO_4 and related Ir^{4+} oxides [1–5]. The atomic Mn/Re moments for the calculation including SOC and Re correlation are $4.17/0.23\ \mu_B$, in good agreement with the experimental values. Concerning the moment directions, the calculated Re moments converged to an antiparallel alignment with respect to the Mn moments for atoms in the same (001) plane, in contrast to the experimentally observed magnetic structure.

IV. DISCUSSION

The magnetic structures displayed in Figs. 2(c) and 2(d) are unusual. Firstly, they show a canting of 21° of the Mn sublattice with respect to a collinear A-AFM structure, while the Re moments make an angle of 100(7)° with respect to the Mn moments at the same z. An attempt to force a collinear magnetic alignment for Mn and Re atoms led to substantially worse fitting quality, and the Re moment converged to zero within statistical error. This analysis reinforced the conclusion that a nearly orthogonal alignment of Mn and Re ions takes place, which is suggestive of dominant antisymmetric (Dzyaloshinskii-Moriya) exchange and/or single ion anisotropy energy contributions in comparison to the symmetric (Heisenberg) exchange that is normally dominant in $3d$ transition metal oxides. This is surprising considering the relatively large value of the magnetic ordering temperature of this material ($T_c = 121$ K), while antisymmetric exchange coupling is normally in the range of 1 K in $3d$ transition-metal compounds. Comparable results with orthogonal Mn and Re moment alignment were reported for the related compound Sr_2MnReO_6 [11,17]. However, FiM contributions to the Bragg peaks are dominant over the A-AFM ones for Sr_2MnReO_6 [11], in opposition to our results for CMRO. Another analog material is the pseudocubic Ba_2MnReO_6, in which Mn moments show a noncollinear structure with a dominant FM component and a canting of 25° between successive (001) planes [19]. This indicates that compounds of this family consistently show largely noncollinear magnetic structures.

Both the experimental data and *ab initio* calculations indicate a dominating weight of the Mn moments in CMRO. On the other hand, in an ionic picture the Mn^{2+} ions with half-filled $3d$ band are isotropic with zero orbital magnetic moments, making the observed canted magnetic structure and magnetic hardness of this material difficult to interpret based upon the Mn moments alone. Thus, the Re $5d$ moments, albeit very weak, must have an important role in the magnetic properties of this material. In fact, the large Re-O hybridization may produce significant orbital polarization also in the oxygen ions that mediate the Mn-Re and Mn-Mn exchange interactions. These ingredients lead to an unusual magnetic structure for

this material that cannot be trivially rationalized in terms of paradigms built upon traditional 3*d* transition-metal magnetism with much weaker effects of relativistic SOC. Further theoretical and experimental investigations are necessary for a deeper understanding of this remarkable behavior.

V. CONCLUSIONS

In summary, neutron diffraction on Ca_2MnReO_6 reveals a noncollinear magnetic structure where the Mn moments are largely canted (21°) and the small Re moments are almost orthogonally aligned with the Mn ones. The large SOC of Re 5*d* electrons is identified as a decisive ingredient leading to the insulating state and the exotic magnetic structure of this material.

ACKNOWLEDGMENTS

Work at UNICAMP was conducted with financial support from FAPESP Grant No. 2012/04870-7, CAPES, and CNPq, Brazil. LLB is acknowledged for concession of beamtime.

APPENDIX: ANALYSIS OF THERMAL NEUTRON POWDER DIFFRACTION DATA

High resolution thermal neutron powder diffraction (t-NPD) measurements were taken at selected temperatures at the 3*T*2 instrument of LLB, adequate for crystal structure investigations, using a vertically focusing Ge(335) monochromator with $\lambda = 1.2292$ Å and a bank of 50 ^{3}He detectors (see Fig. 5). We employed 10′ in-pile collimation upstream the monochromator and 10′ Soller collimators in front of the 50 counters. Contrary to the c-NPD data displayed in the main text, which were collected ∼6 months after the synthesis with the sample being kept in an inert He atmosphere during this time interval, the t-NPD data were only taken after two years of sample exposure to ambient atmosphere. As an unwanted consequence of this time lapse between the experiments, unidentified impurity peaks were clearly observed at 1.62, 2.07, and 2.21 Å^{-1} in the t-NPD data, which likely arise from grain boundary carbonation. Still, satisfactory fitting quality was achieved when these impurities peaks were excluded from the refinement. The refined lattice parameters of the main phase are consistent with those obtained from the c-NPD data and the refined Mn/Re intersite disorder for the t-NPD data is 2.9(5)%, slightly larger than 0.6(7)% obtained from the c-NPD data, indicating only minor deterioration of the ordered double perovskite main phase in the time lapse between these experiments. Table I shows the refined atomic parameters at the investigated temperatures. The extracted (Mn,Re)-O bond lengths and Mn-O-Re bond angles are shown in Table II.

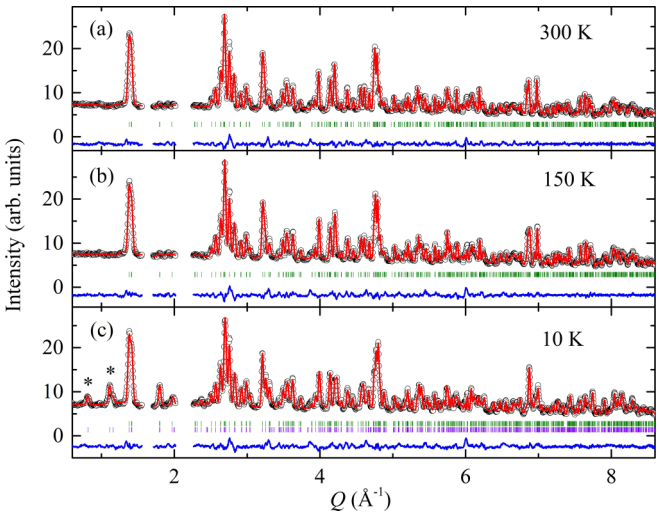

FIG. 5. Experimental (symbols) and calculated (red lines) thermal neutron powder diffraction profile of Ca_2MnReO_6 at 300 K (a), 150 K (b), and 10 K (c). The difference curves (blue solid line) are displayed at the bottom of each figure. The reflection positions are indicated in short vertical lines for both the nuclear [(a), (b), and (c)] and magnetic [(c), lower vertical lines] structures. Stars represent purely magnetic peaks.

[1] B. J. Kim, H. Jin, S. J. Moon, J.-Y. Kim, B.-G. Park, C. S. Leem, J. Yu, T. W. Noh, C. Kim, S.-J. Oh, J.-H. Park, V. Durairaj, G. Cao, and E. Rotenberg, Phys. Rev. Lett. **101**, 076402 (2008).
[2] B. J. Kim, H. Ohsumi, T. Komesu, S. Sakai, T. Morita, H. Takagi, and T. Arima, Science **323**, 1329 (2009).
[3] D. Pesin and L. Balents, Nat. Phys. **6**, 376 (2010).
[4] G. Cao and P. Schlottmann, Rep. Prog. Phys. **81**, 042502 (2018).
[5] G. Jackeli and G. Khaliullin, Phys. Rev. Lett. **102**, 017205 (2009).
[6] H. Kato, T. Okuda, Y. Okimoto, Y. Tomioka, K. Oikawa, T. Kamiyama, and Y. Tokura, Phys. Rev. B **69**, 184412 (2004).
[7] H. P. S. Corrêa, I. P. Cavalcante, D. O. Souza, E. Z. Santos, M. T. D. Orlando, H. Belich, F. J. Silva, E. F. Medeiro, J. M. Pires, J. L. Passamai, L. G. Martinez, and J. L. Rossi, Cerâmica **56**, 193 (2010).
[8] J. B. Depianti, M. T. D. Orlando, A. S. Cavichini, H. P. S. Corrêa, V. A. Rodrigues, J. L. Passamai, E. L. O. Piedade, H. Belich, E. F. Medeiros, and F. C. L. de Melo, Cerâmica **59**, 262 (2013).
[9] J. Rodríguez-Carvajal, Physica B **192**, 55 (1993).
[10] A. C. Larson and R. B. Von Dreele, Los Alamos National Laboratory Report LAUR 86-748 (2000); B. H. Toby, J. Appl. Cryst. **34**, 210 (2001).
[11] G. Popov, M. V. Lobanov, E. V. Tsiper, M. Greenblatt, E. N. Caspi, A. Borissov, V. Kiryukhin, and J. W. Lynn, J. Phys.: Condens. Matter **16**, 135 (2004).
[12] P. Giannozzi, S. Baroni, N. Bonini, M. Calandra, R. Car, C. Cavazzoni, D. Ceresoli, G. L. Chiarotti, M. Cococcioni, I. Dabo, A. Dal Corso, S. Fabris, G. Fratesi, S. de Gironcoli, R. Gebauer, U. Gerstmann, C. Gougoussis, A. Kokalj, M. Lazzeri,

L. Martin-Samos, N. Marzari, F. Mauri, R. Mazzarello, S. Paolini, A. Pasquarello, L. Paulatto, C. Sbraccia, S. Scandolo, G. Sclauzero, A. P. Seitsonen, A. Smogunov, P. Umari, and R. M. Wentzcovitch, J. Phys.: Condens. Matter **21**, 395502 (2009).

[13] J. P. Perdew, K. Burke, and M. Ernzerhof, Phys. Rev. Lett. **77**, 3865 (1996).

[14] P. E. Blöchl, Phys. Rev. B **50**, 17953 (1994); G. Kresse and D. Joubert, *ibid.* **59**, 1758 (1999).

[15] We used the files Ca.pbe–spn–kjpaw_psl.1.0.0.UPF, Mn.pbe–spn–kjpaw_psl.1.0.0.UPF, Re.rel–pbe–spfn–kjpaw_psl.1.0.0.UPF, and O.pbe–nl–kjpaw_psl.1.0.0.UPF available at http://people.sissa.it/-pl2X-sim-dalcorso/pslibrary/index.html.

[16] B. D. Cullity and C. D. Graham, *Introduction to Magnetic Materials*, 2nd ed. (John Wiley and Sons, Inc., Hoboken, NJ, 2009).

[17] G. Popov, M. Greenblatt, and M. Croft, Phys. Rev. B **67**, 024406 (2003).

[18] V. I. Anisimov, J. Zaanen, and O. K. Andersen, Phys. Rev. B **44**, 943 (1991).

[19] C. P. Khattak, D. E. Cox, and F. F. Y. Wang, J. Sol. State Chem. **13**, 77 (1975).